

Brain Tumor Diagnosis Using Quantum Convolutional Neural Networks

Muhammad Al-Zafar Khan^{¶||}, Nouhaila Innan^{†*}, Abdullah Al Omar Galib^{§†}, Mohamed Bennai^{¶**}

[¶]Quantum United Arab Emirates (QUAE), UAE

[†]Quantum Physics and Magnetism Team, LPMC, Faculty of Sciences Ben M'sick,
Hassan II University of Casablanca, Morocco

[§]Independent Researcher

^{||}m.khan@quae.ae, ^{*}nouhaila.innan-etu@etu.univh2c.ma, [†]abdullahalomargalib@gmail.com, ^{**}mohamed.bennai@univh2c.ma

Abstract—Integrating Quantum Convolutional Neural Networks (QCNNs) into medical diagnostics represents a transformative advancement in the classification of brain tumors. This research details a high-precision design and execution of a QCNN model specifically tailored to identify and classify brain cancer images. Our proposed QCNN architecture and algorithm have achieved an exceptional classification accuracy of 99.67%, demonstrating the model's potential as a powerful tool for clinical applications. The remarkable performance of our model underscores its capability to facilitate rapid and reliable brain tumor diagnoses, potentially streamlining the decision-making process in treatment planning. These findings strongly support the further investigation and application of quantum computing and quantum machine learning methodologies in medical imaging, suggesting a future where quantum-enhanced diagnostics could significantly elevate the standard of patient care and treatment outcomes.

Index Terms—Quantum Convolutional Neural Networks, Convolutional Neural Networks, Quantum Machine Learning, Quantum Computing

I. INTRODUCTION

Brain tumors are neoplasms that represent abnormal cell growth within the brain and its surrounding structure. Although a relatively rare form of cancer – in comparison to other cancers – analogous to other cancers, it can be benign or malignant. It is poorly diagnosed because neurological symptoms cannot be detected easily, and specific tests, like biopsies and analysis of brain scans, need to be conducted by human experts. The process of diagnosis usually involves three facets: Consideration of molecular features, analysis of histological characteristics (microscopic analysis of cells and tissues from the brain), and anatomical location (lobes of the brain).

Holistically, these tumors are categorized as follows:

- 1) **Meningiomas:** Tumors originating from the meninges surrounding the brain and the spinal cord,
- 2) **Pituitary Adenomas:** Tumors originate in the pituitary gland at the base of the brain.
- 3) **Gliomas:** Tumors that originate from the glial cells in the central nervous system. Gliomas are the most common type of brain tumors that are developed, and are therefore known as “primary brain tumors.”
- 4) **Metastatic Lesions:** Tumors originate from cancer cells in other parts of the body, and have spread via metastasis to the brain. Therefore, they are known as “secondary brain tumors”.

- 5) **Medulloblastomas:** Tumors that originate from the cerebellum, and are most commonly found in children.
- 6) **Acoustic Neuromas / Schwannomas:** Tumors that originate from the Schwann cells insulting nerve fibers.
- 7) **Pinealomas / Pineocytoma:** Tumors that originate from the pineal gland.

According to research published by the American Cancer Society [1], in 2023 for the state of Ohio in the United States, it was reported that 24 810 adults (with 14 280 being men, and 10 530 being women) in the United States were diagnosed with a form of cancerous tumors of the brain and spinal cord, and a 2020 survey found that globally 308 102 people were diagnosed. Although a small percentage of the overall population of the United States and the world, respectively, these patients are eligible to receive the best care possible.

Usually, treatment paths are patient-specific, depending on several factors, such as the patient's current state of health, the presence of other underlying diseases, and so on. As with other cancers, treatment is very expensive, and requires the patient to take significant steps to a complete lifestyle overhaul. This diverse approach encompasses, amongst others, a change of diet, incorporation of exercise, radiation therapy, immunotherapy, chemotherapy, and molecular therapy.

With the current Artificial Intelligence (AI) revolution in all fields that the world is experiencing, the medical field is no exception. Specifically, within the context of the analysis of medical images for diagnosis and prognosis, Convolutional Neural Networks (CNNs) are a type of NN architecture designed for computer vision and image processing assignments. Similar to how a perceptron is modeled after biological neurons, the CNN is modeled after the cortical preprocessing regions of the striate cortex (primary visual cortex – V1) and the prostrate cortex (secondary visual cortex – V2), located at the occipital lobe at the back of the brain. Analogous to how computer vision tasks in the pre-Machine Learning (ML) and pre-Deep Learning (DL) eras used to be concerned with detecting edges, shapes, and textures, the neurons in this region are sensitive to discerning these patterns. CNNs have proven to be invaluable in the medical domain, and many healthcare facilities are incorporating CNN-based classification systems together with medical experts for early disease detection, and recommended treatment plans [2]–[4].

Architecturally, the CNN is described as being composed of two distinguishable layers:

- 1) **Convolutional Layer:** These contain adjustable fil-

ters/kernels/weights optimized for the task’s superlative performance. The output from this layer is known as *feature maps*. Given a two-dimensional input image X , the kernel K is applied in order to get the feature map Y at each spatial location

$$Y(i, j) = \sum_m \sum_n X(i + m, j + n) \cdot K(m, n), \quad (1)$$

where i and m are the x -coordinates of the image and kernel locations respectively, and j and n are the y -coordinates image and kernel locations respectively. Subsequently, a nonlinear activation function that serves the network in order to introduce sparsity into the network, mitigate small gradients so that the vanishing gradients problem is avoided during backpropagation, and speed up the convergence of the loss function. Typically in a CNN, a $\text{ReLU}(x) = \max(0, x)$, or a variant, is used.

2) **Pooling Layer/Max Pooling/Subsampling:** These reduce the spatial resolution of the feature maps by a process called *downsampling*, which reduces the size of the feature map, typically by half its original size. There are several types of pooling operations, these include:

a) **Max Pooling:** Chooses the maximum value from each subregion of the feature map.

$$Y(i, j) = \max_{m, n} X(i \times s + m, j \times s + n), \quad (2)$$

where s is the *stride* or number of pixel shifts over the input matrix.

b) **Average Pooling:** Chooses the average value from each subregion of the feature map.

$$Y(i, j) = \frac{1}{k} \sum_m \sum_n X(i \times s + m, j \times s + n). \quad (3)$$

c) **ℓ^2 Norm Pooling:** Chooses the ℓ^2 norm of each subregion in the feature map.

$$Y(i, j) = \frac{1}{k} \sum_m \sum_n X^2(i \times s + m, j \times s + n). \quad (4)$$

d) **Global Pooling:** Chooses the maximum or average value across all the feature maps in a layer. This produces a single scalar value for each feature map.

Subsequently, once a series of convolution and pooling layers are applied (the number of each is an adjustable hyperparameter decided to maximize accuracy, and minimize time to convergence), the output is flattened, and fed to the terminal layer, where classification takes place. Generally, the sigmoid, $\sigma(x) = 1/[1 + \exp(-x)]$, function is used for binary classification tasks, or the softmax, $\tilde{\sigma}(\mathbf{x}) = \exp(x_i) / \sum_{j=1}^{|\text{classes}|} \exp(x_j)$, is used, where $|\text{classes}|$ is the number of classes.

Furthermore, the sub-operations within the network that take place include:

Subsampling decreases the number of weights in the network, thereby increasing the receptive field of the neurons in

order to capture more information about the input image on a global scale, and improve the network’s ability to recognize objects, no matter their location via *translational invariance*.

Convolution is the mathematical operation of sliding a filter matrix, containing learnable weights that help infer different features over the image and take the inner product of the matrix with the pixel at each location to extract the feature. The importance of convolution cannot be over-stressed as it is fundamental for automatically discerning features, thus eliminating the need for manual feature engineering. However, each time a convolutional operator is applied, the dimensionality of the image is reduced.

Padding is the process of adding pixels around the edge of an image prior to applying the convolutional operator. This process is vital because it ensures that the resulting feature map has the same dimensions as the input image. In addition, if images are not edge-pixelated, once the convolutional operator is applied.

Batch normalization is a statistical technique used to normalize the activations of the neurons in the CNN. This is accomplished by adjusting and scaling the inputs to each layer.

However, classical CNNs have the drawback of being unable to learn global and remote semantic information well, amongst others. Therefore, a natural consideration for advancement would be the incorporation of another thriving technology; thus, our proposal of supplementation via Quantum Machine Learning (QML). Below we summarize the drawbacks of classical CNNs, and highlight how QCCNs may conceivably address these challenges.

1) **The Problem of Overfitting:** CNNs are highly prone to learning the probability distributions of the training data “too well”, and therefore even learn erroneous noise and outliers. **Owing to larger feature spaces, QCNNs are potentially less prone to overfitting.**

2) **Cost of Computation:** Regular CNNs have quadratic runtimes, $\mathcal{O}(\mathcal{N}_i \times \mathcal{N}_o^2 \times \mathcal{S}_i^2 \times \mathcal{S}_c^2)$, where \mathcal{N}_i is the number of input feature maps, \mathcal{N}_o is the number of output feature maps, \mathcal{S}_i is the size of the input feature map, and \mathcal{S}_c is the size of the convolution filter. **QCNNs have the potential to be much lower due to the superposition of qubits that create an exponential speedup.**

3) **Learning Mappings from Features to the Predictor:** As the image dataset gets more complicated, and more expansive in size, CNNs limited in their expressivity. **QCNNs have the potential to be more expressive due to exploiting the quantum mechanical properties of superposition and entanglement.**

Therefore, it is evident that considering QCNNs, and the augmentation of classical CNNs with QML proves to be a fruitful venture. Integrally, QML is a developing research enterprise, that has myriad real-world applications in diverse fields like drug discovery [5]–[9], materials science [10], [11], condensed matter physics [12]–[15], optimization [16]–[20], finance [21]–[25], logistics planning [26]–[29], cryptography

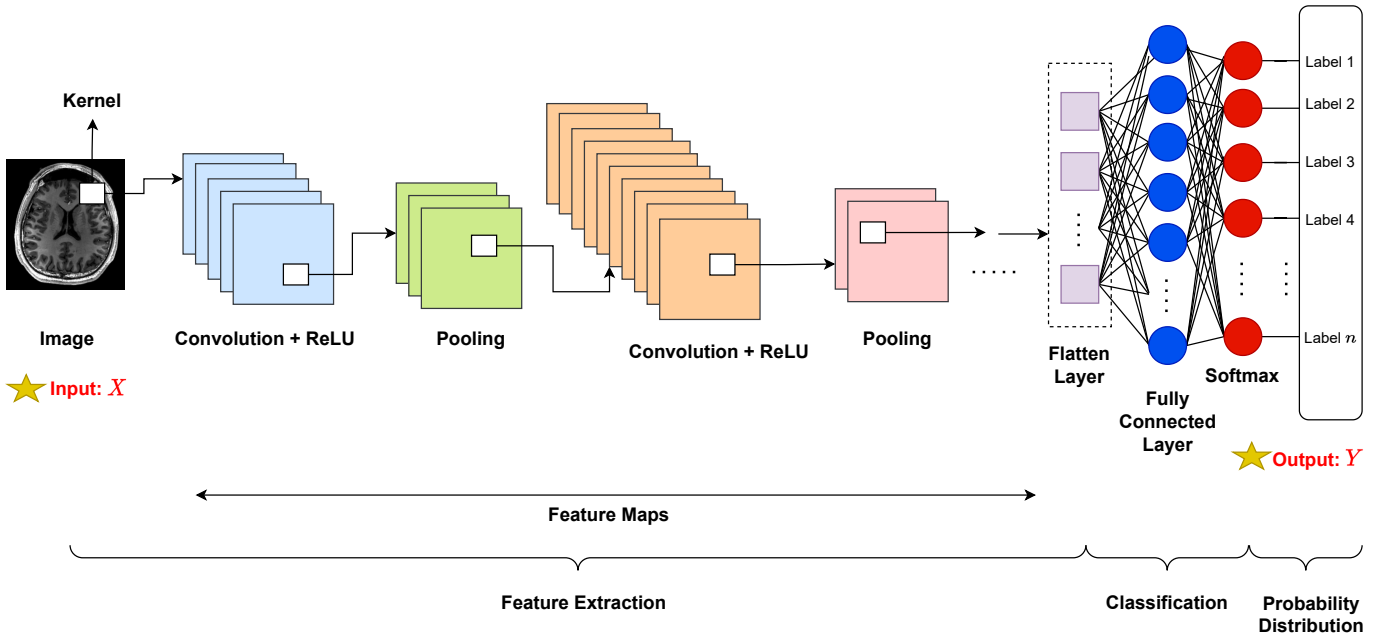


Fig. 1: Architecture of a classical CNN.

and cybersecurity [30], [31], and many other innovative applications [32]–[35].

The augmentation of QML with CNNs leads to *Quantum Convolutional Neural Networks* (QCNNs). In this study, we use QCNNs to perform brain tumor classifications on an open-source brain tumor image dataset. While this is not novel, this study offers several contemporary advancements, and superior performance for in-distribution classification, as well as out-of-distribution generalizability.

The original contributions of this paper are: The integration of an extremely large image dataset, which is significant considering the computational power available in the NISQ era; the development and implementation of a QCNN with a classical component that achieves high accuracy; and a modular and scalable framework for the QCNN that ensures adaptability to various computational contexts.

The structure of this paper is organized in the following manner:

In Sec. II, we provide a literature review of the most relevant papers in the field.

In Sec. III, we delve into the methodologies and underlying theories of QCNNs, providing a detailed theoretical background.

In Sec. IV, we describe the process and implementation of the QCNN used in this study, detailing the adaptations and enhancements made to the original model.

In Sec. V, we present the results of our experiments.

In Sec. VI, we summarize our research findings and provide a reflective analysis of the results obtained.

II. LITERATURE REVIEW

Below, we present salient studies that have motivated our research undertaking, that have applied QML to brain tumor

classification tasks, and briefly describe the results obtained.

In [36], the authors developed a hybrid quantum-classical CNN (HQC-CNN) model for brain tumor classification. The novelties of the proposed network were that it achieved a high classification score (97.8%), it was easy to train, and it converged to a solution very quickly. The classification problem was posed as a quaternary model, i.e., having four output class types: Meningioma, glioma, pituitary, and no tumor. In addition, it was demonstrated that the proposed network outperformed many well-known models.

In [37], the authors use deep features extracted from the famous Inception v3 model, combined with a parametric quantum circuit on a predictor variable with four classes, similar to the classification task in [36]. Using three datasets as benchmarks (from Kaggle, the 2020-BRATS dataset, and locally-collected dataset), it was shown that the hybrid approach proposed here should have superior performance compared to traditional CNNs, with more than 90% accuracy.

The research in [38] sets out to address the ever-growing size of image datasets in medical diagnosis while maintaining patient privacy, with a specific emphasis on brain tumor images. Further, a secure encryption-decryption framework is designed to work on Magnetic Resonance Imaging (MRI) data, and a 2-qubit tumor classification model is implemented. The Dice Similarity Coefficient (DSC) was used as a validation metric, and the model was found to have a value of 98%. This research not only considered designing a high-accuracy brain tumor classification model but also addressed the issue of cryptographic concerns.

In [39], the authors aim to address concerns around tumor imaging and prediction using traditional ML techniques amongst children and teenagers. Using India as a study group,

it is found that the data lacks variability, and does not account for abnormalities within these specific groups. To address this, a QCNN model is proposed that integrates techniques from image processing to mitigate noise. It is found that the proposed quantum network achieves an 88.7% accuracy.

In [40], the authors use the MRI dataset to implement a brain tumor model using an MRI-radiomics variational Quantum Neural Network (QNN). The workflow involved the usage of a mutual information feature selection (MIFS) technique, and the problem was converted into a combinatorial optimization task, which was subsequently solved using a quantum annealer on a D-Wave machine. While specifically not a CNN-based model, or augmentation thereof, the technique proved versatile and achieved on-par accuracies with classical methods.

In [41], the authors design an automatic MRI segmentation model based on qutrits (quantum states of the form $|\psi\rangle = \alpha|0\rangle + \beta|1\rangle + \gamma|2\rangle$ with $|\alpha|^2 + |\beta|^2 + |\gamma|^2 = 1$), called *quantum fully self-supervised neural networks* (QFS-Net). It is shown that this approach increases segmentation accuracy (model predictability) – outperforming classical networks – and convergence. Besides using a qutrit framework for which the model is based, the other novel contributions of this research were the implementation of parametrized Hadamard gates, the neighborhood-based topological interconnectivity amongst network layers, and the usage of nonlinear transformations. It was demonstrated that QFS-Net showed favorable results on the Berkeley gray-scale images.

Various other literature pieces are contained within the pieces discussed above, and it will be an exercise in futility simply to repeat the findings. However, what is evident is that the hybrid approach, via augmentation of the QCNN with salient features of the classical CNN, emphasized in the literature, serves as motivation for adopting a hybridized approach to the network in this paper.

III. METHODOLOGY

In this section, we present the mathematical formalism of QCNNs.

Comparably similar to CNNs, QNNs use a network of quantum convolution layers and quantum activation functions to perform feature extraction from images. Operationally, as presented in Fig. 2, we can describe the operation of a QCNN as follows:

- 1) **Data Encoding:** Classical data $D_i \in \mathcal{D}$ is converted to a single-qubit quantum state $|\psi_i\rangle \in \mathcal{H}$,

$$D_i \xrightarrow{\text{encoding}} |\psi_i\rangle = \alpha|0\rangle + \beta|1\rangle, \quad (5)$$

where $\alpha, \beta \in \mathbb{C}$ are complex probability amplitudes.

- 2) **Quantum Convolution:** This is achieved by applying a series of quantum gates to the encoded state $|\psi\rangle$. We cumulatively represent these gates as U_* ,

$$U_* |\psi\rangle = U_* \triangleq \text{combination}(H^{\otimes n_1}, R_\theta^{\otimes n_2}, X^{\otimes n_3}, Y^{\otimes n_4}, Z^{\otimes n_5}, \dots), \quad (6)$$

where the function `combination` represents taking amalgamations of the single-qubit gates for n_i , and $i = 1, 2, \dots$, number of times.

- 3) **Quantum Pooling:** The operation is carried out by performing the *quantum SWAP test*: Given two quantum states $|\psi_i\rangle, |\psi_j\rangle$ and an ancillary qubit $|0\rangle$,

- 3.1. Apply the Hadamard gate to the ancillary qubit in order to create a superposition

$$H|0\rangle = \frac{1}{\sqrt{2}}(|0\rangle + |1\rangle) = |+\rangle. \quad (7)$$

- 3.2. Apply the controlled-SWAP gate with $|0\rangle$ as the control, and $|\psi_i\rangle$ and $|\psi_j\rangle$ as the targets,

$$\begin{aligned} \text{CSWAP}(|0\rangle; |\psi_i\rangle, |\psi_j\rangle) = & |0\rangle\langle 0| \otimes |\psi_i\rangle\langle \psi_i| \\ & + |1\rangle\langle 1| \otimes |\psi_j\rangle\langle \psi_j|. \end{aligned} \quad (8)$$

- 3.3 Apply the Hadamard transformation,

$$H|0\rangle = |+\rangle.$$

- 4) **Fully-Connected Layer:** This layer is composed of neurons that are oriented in a feed-forward arrangement whereby previous neurons are connected to all subsequent neurons.

- 5) **Measurement:** Perform measurement to ascertain the end state.

In Algorithm 1, we provide a general procedure for applying the QCNNs model to any dataset.

Algorithm 1 QCNN(\mathcal{D})

procedure QCNN(\mathcal{D})

Input: a dataset $\mathcal{D} = \{D_1, D_2, \dots, D_p\}$ consisting of $p \times n \times m$ -dimensional images

Initialize the number of repeats q for the quantum convolutional and quantum pooling layers

for each image D_i in \mathcal{D} **do**

Encode D_i into quantum state $|\psi_i\rangle$

repeat

Apply U_* ,

Measure

Apply quantum SWAP test

until q times

end for

Apply a fully connected NN to transform the output into a 1D vector of class scores

Measure to obtain classifications

Return classified image with associated probability

end procedure

IV. PROCESS AND IMPLEMENTATION

In this section, we detail the practical steps taken to operationalize our QCNN model by discussing the workflow. We begin by delineating the composition and sourcing of our dataset, followed by the procedures employed in data preprocessing to

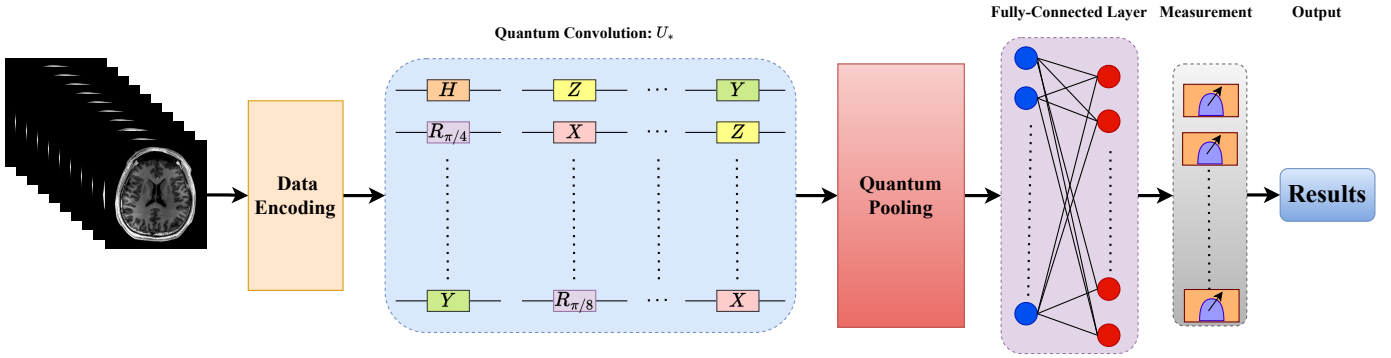


Fig. 2: Hypothetical architecture of QCNNs model.

ensure optimal model input quality. Subsequently, we elucidate our innovative approach to quantum image processing, which sets the stage for the subsequent CNN training. This phase is critical as it underpins the model’s ability to learn from the quantum-enhanced feature space. Each step is crafted to build incrementally towards a robust and practical QCNN application.

A. Dataset

The dataset used in this research [42] comprises 3 064 T1-weighted contrast-enhanced images extracted from 233 patients, encompassing three distinct brain tumor types, as shown in Fig. 3: meningioma (708 slices), glioma (1 426 slices), and pituitary tumor (930 slices). The data is organized in MATLAB format (.mat files), each containing a structure that encapsulates various fields detailing the image and tumor-specific information. Each MATLAB (.mat) file in the dataset encompasses the following key fields:

- a. `cjdata.label`: An integer indicating the tumor type, coded as follows:
 - 1) Meningioma
 - 2) Glioma
 - 3) Pituitary Tumor

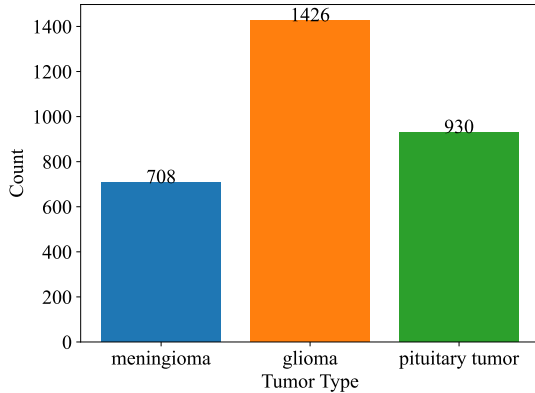


Fig. 3: Distribution of sample sizes across tumor categories in the dataset.

- b. `cjdata.PID`: Patient ID, serving as a unique identifier for each patient.
- c. `cjdata.image`: Image data representing the T1-weighted contrast-enhanced brain scan.
- d. `cjdata.tumorBorder`: A vector storing the coordinates of discrete points delineating the tumor border. The vector format is as follows:
 - $[x_1, y_1, x_2, y_2, \dots]$
 - These coordinate pairs represent planar positions on the tumor border and were generated through manual delineation, offering the potential to create a binary image of the tumor mask.
- e. `cjdata.tumorMask`: A binary image where pixels with a value of 1 signify the tumor region. This mask is a crucial resource for further segmentation and analysis.

This dataset provides a diverse set of brain scans, as shown in Fig. 4, and includes manual annotations of tumor borders, fostering the development and evaluation of robust image processing and ML models for brain cancer classification [43], [44].

B. Data Preprocessing

This step loads the MATLAB data files and extracts image data, tumor labels, and relevant information. Then, it converts the T1-weighted images to a format suitable for quantum circuit processing.

C. Quantum Image Processing

In this step, the QCNN circuit stands as a pivotal component, and the circuit comprises several essential elements. Initially, a quantum device with four qubits initializes using PennyLane’s default qubit simulator [45], as presented in Fig. 5. A significant step in this process is setting the parameter θ to $\pi/2$. This parameter finds its application in Controlled-Rotation-Z (CR_Z) and Controlled-Rotation-X (CR_X) gates. The circuit employs Rotation-X (R_X) gates applied to each qubit. These gates rotate the qubit around the X-axis of the Bloch sphere. The rotation angle is proportional to the pixel value times π . This operation is mathematically expressed as

$$|\psi'\rangle = \bigotimes_{i=0}^3 R_X(\phi_i \pi) |\psi\rangle, \quad (9)$$

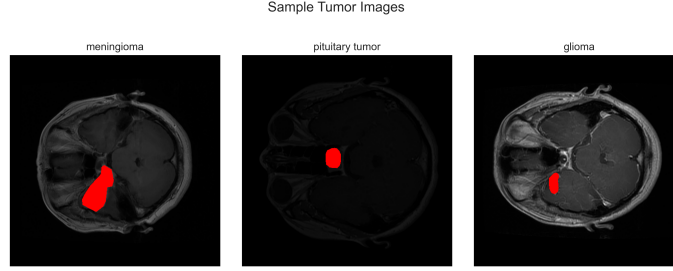


Fig. 4: Diagnostic imaging examples: Brain tumor types from the dataset.

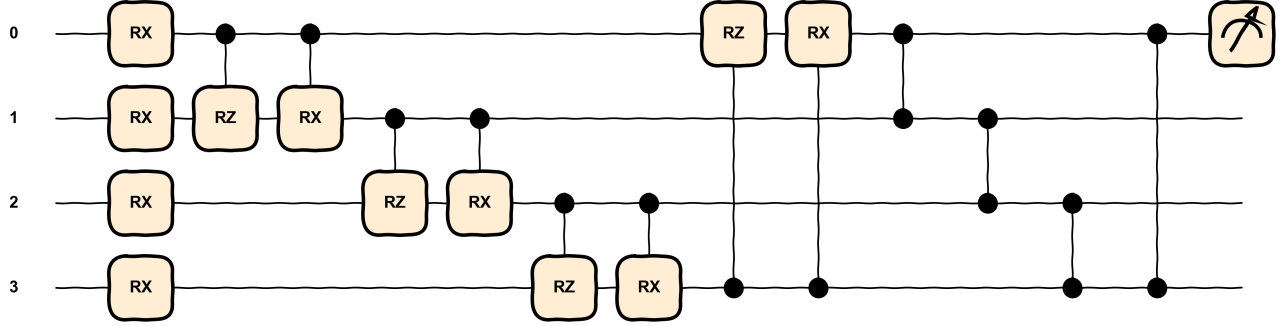


Fig. 5: QCNN circuit.

with

$$R_X(\phi_i\pi) = \begin{pmatrix} \cos \phi_i\pi/2 & -i \sin \phi_i\pi/2 \\ -i \sin \phi_i(\pi/2) & \cos \phi_i\pi/2 \end{pmatrix}, \quad (10)$$

where $|\psi\rangle = |0\rangle^{\otimes 4}$ represents the initial state of the quantum system, and ϕ_i are the elements of the pixel value array passed to the quantum circuit.

Following this, the circuit incorporates controlled rotation gates, specifically CR_Z and CR_X gates. These gates are applied between each pair of adjacent qubits and between the last and first qubits. These gates introduce interactions between the qubits. Mathematically, this is represented as

$$|\psi''\rangle = (CR_Z(\theta)_{0,1} \cdot CR_X(\theta)_{0,1}) \times (CR_Z(\theta)_{1,2} \cdot CR_X(\theta)_{1,2}) \times (CR_Z(\theta)_{2,3} \cdot CR_X(\theta)_{2,3}) |\psi'\rangle \quad (11)$$

with

$$CR_Z(\theta) = \begin{pmatrix} 1 & 0 & 0 & 0 \\ 0 & 1 & 0 & 0 \\ 0 & 0 & \exp(-i\theta/2) & 0 \\ 0 & 0 & 0 & \exp(i\theta/2) \end{pmatrix}, \quad (12)$$

and

$$CR_X(\theta) = \begin{pmatrix} 1 & 0 & 0 & 0 \\ 0 & 1 & 0 & 0 \\ 0 & 0 & \cos \theta/2 & -i \sin \theta/2 \\ 0 & 0 & -i \sin \theta/2 & \cos \theta/2 \end{pmatrix}, \quad (13)$$

where $CR_Z(\theta)$ and $CR_X(\theta)$ are the phase-parameterized CR_Z and CR_X gates, respectively. Moreover, the circuit incorporates CZ gates that are applied between each pair of adjacent qubits, and between the last and first qubits, we add an additional layer of entanglement between the qubits; mathematically, this is represented as

$$|\psi'''\rangle = CZ_{0,1} \cdot CZ_{1,2} \cdot CZ_{2,3} \cdot CZ_{3,0} |\psi''\rangle \quad (14)$$

with

$$CZ = \begin{pmatrix} 1 & 0 & 0 & 0 \\ 0 & 1 & 0 & 0 \\ 0 & 0 & 1 & 0 \\ 0 & 0 & 0 & -1 \end{pmatrix}, \quad (15)$$

Finally, the measurement phase occurs. In this phase, the expectation value of the Pauli-Z operator is measured on the first qubit. This step provides the average result of numerous measurements, mathematically encapsulated as

$$\mathcal{M} = \langle \phi'''' | Z | \phi'''' \rangle, \quad (16)$$

where $|\phi''''\rangle$ is the state after the CZ gates, indicating the output of the quantum convolution operation on the 2×2

patch as a complex function of the pixel values, reflective of the quantum nature of the operation.

The quantum convolution function plays a crucial role in the process of quantum image processing. This function is designed to perform a quantum convolution operation on an input image. The function requires two arguments: Firstly, an image represented as a 2D NumPy array, where each element corresponds to a pixel value. Secondly, the step size, which divides the image into patches, is set to 2 by default. Thus, the image is divided into 2×2 patches.

In terms of processing, the function begins by initializing a new 2D array of zeros. The dimensions of this array are determined by the height and width of the image divided by the step size, and this array serves to store the output of the quantum convolution operation. Subsequently, the function divides the image into 2×2 patches by looping over the image with the specified step size. For each 2×2 patch, the function flattens the patch into a 1D array and then applies the quantum convolution operation, as performed by the QCNN circuit. The measurement result of this operation is then stored in the corresponding position in the output array.

In the output layer, the function returns a new 2D array. Each element in the array represents the result of the quantum convolution operation on the corresponding 2×2 patch in the original image. This resulting array can be perceived as a transformed version of the original image, where the transformation is a complex function of the pixel values stemming from the quantum nature of the operation.

The core component of the implementation is a loop designed for image processing, which iterates through every file in a designated folder, provided that the current file has been processed during each iteration. If it has not, it loads the image and its associated label from the file. Following this, it resizes and normalizes the image. Subsequently, a quantum convolution function is applied to the image. Finally, the processed image and its label are saved into a new file.

D. CNN Training

This approach involves training the CNN on quantum-processed image data. The model architecture comprises various layers, each with specific functions. The first is a Conv2D layer with 32 filters, a 3×3 kernel size, and ReLU activation, designed to detect low-level features like edges and corners in the input image. This is followed by a MaxPooling2D layer with a 2×2 pool size, which reduces the spatial dimensions of the input by taking the maximum value in each 2×2 window, aiding in translation invariance and reducing computational complexity. Another Conv2D layer is then applied, with 64 filters, and once again with ReLU activation, to detect more complex features from the previous layer's output. A second MaxPooling2D layer further reduces the input's spatial dimensions. The flatten layer then converts the 2D output into a 1D array for processing in the dense layers. Subsequently, a dense layer with 128 units and ReLU activation learns to represent the input in a 128-dimensional space, detecting high-level features. To prevent overfitting, a dropout layer with

a 0.5 dropout rate is included, randomly setting half of the input units to 0 during training. Finally, another dense layer with four units and softmax activation outputs the probabilities of the input image belonging to each of the four classes. This comprehensive architecture enables the classical CNN to effectively learn from the quantum-processed data.

V. RESULTS AND DISCUSSION

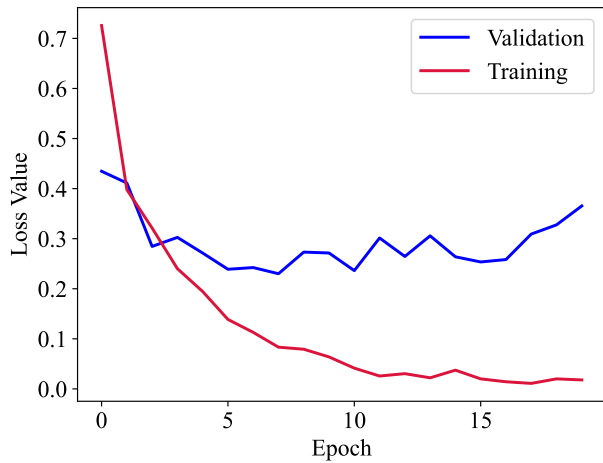
This study thoroughly examined the application of a type QCNN for classifying brain tumor images for the purpose of having a more expressive model that can be used in diagnostic medicine. The performance metrics from our findings highlight the model's exceptional accuracy and potential application for commercialization and usage in a real-world setting.

The loss and accuracy were calculated for 20 epochs for the training and validation data. As presented in Fig. 6a, the progressive decline in loss indicates the model's robust error minimization capabilities. This steady reduction in training and validation loss signifies that the QCNN model is effectively learning from the training data while also generalizing well to new, unseen data. Such a trend strongly indicates the model's ability to avoid overfitting, a common challenge in deep learning models applied to medical image analysis.

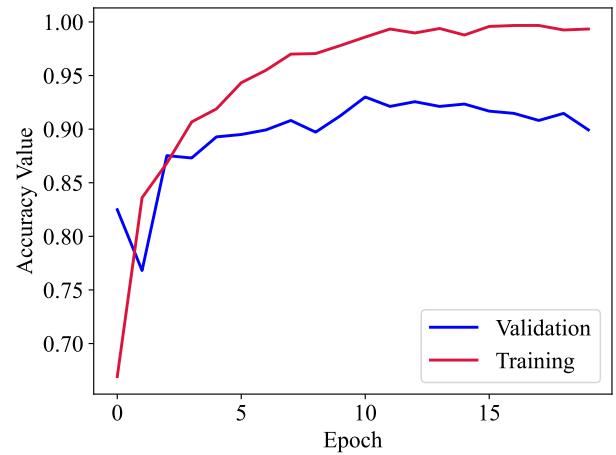
Similarly, the consistent increase in accuracy shown in Fig. 6b confirms the model's competence in correctly classifying brain tumors. The high accuracy rate, especially with a peak validation accuracy of 99.67% is particularly noteworthy given the complexity and variability inherent in medical imaging data. This suggests that the QCNN can capture intricate patterns and features in the images, which are crucial for accurate diagnosis. However, it is crucial to note that performance may vary with changes in image complexity and dataset diversity.

The confusion matrix, shown in Fig. 7, offers additional insights into the model's performance, particularly in its class-wise accuracy. The perfect classification of "pituitary tumor" cases is a testament to the model's precision. However, there are challenges observed in differentiating between the meningioma and glioma classes. This highlights areas for further refinement. These misclassifications may stem from the inherent similarities in the imaging characteristics of these tumor types, suggesting a need for more nuanced feature extraction techniques or additional training data to enhance differentiation. The practical utility of the QCNN model is further validated through the real-world test cases showcased in Fig. 8, which displays 10 randomly selected test images, each annotated with its actual label and the model's prediction. The accurate predictions in these cases demonstrate the model's readiness for deployment in clinical settings, where it can aid in the rapid and reliable diagnosis of brain tumors.

In summary, the QCNN model's outstanding performance in this study demonstrates its capability as a powerful analytical tool in medical imaging and highlights its transformative potential in clinical diagnostics. The model's high accuracy, achieved in the challenging task of brain tumor image classification, underscores its precision and reliability. Moreover, the robustness of the QCNN in processing and interpreting



(a)



(b)

Fig. 6: Training and validation performance plots: (a) Loss and (b) Accuracy.

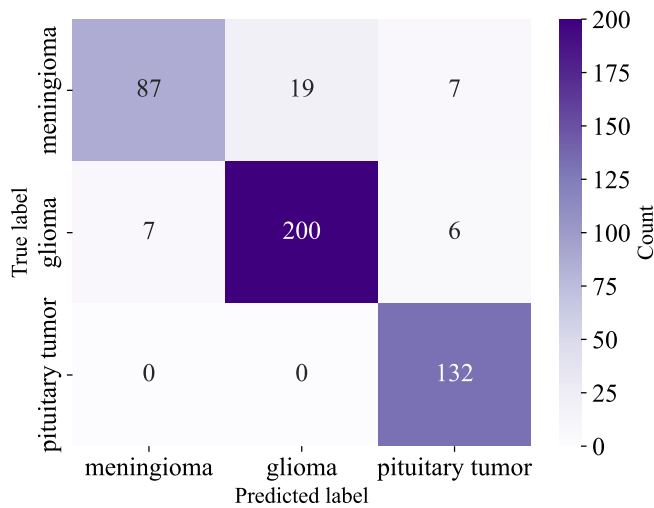


Fig. 7: Confusion matrix displaying class-wise performance.

complex image data attests to its sophisticated design and adaptability. This robustness is particularly crucial in medical imaging, where image variability and accuracy are paramount.

The QCNN model's ability to consistently improve over training epochs, as evidenced by decreasing loss and increasing accuracy, indicates a strong learning capability and a practical approach to generalizing from training data to unseen data. This aspect is vital for clinical applications where models must perform reliably on diverse and novel datasets. Furthermore, despite some challenges, the model's nuanced handling of different tumor types opens avenues for further optimization and rarefaction. These qualities collectively position the QCNN model as a promising candidate for real-world clinical applications, potentially revolutionizing how medical imaging is analyzed and interpreted.

VI. CONCLUSION

This paper presents a comprehensive exploration of QCNNs in the context of medical imaging, particularly for brain tumor classification. A theoretical overview of QCNNs and conventional CNNs was provided, followed by a detailed literature review of various approaches in this domain. This theoretical groundwork laid the foundation for our practical implementation, which introduced innovative modifications while adhering to general QCNN principles.

Our implementation strategy involved integrating a conventional CNN within the QCNN framework, essentially creating a hybrid model that leverages both technologies' strengths. This approach deviates from standard QCNN designs and represents an experimental foray into uncharted territories of neural network architectures.

Additionally, using a quantum simulator to execute the model and generate results is a significant step in practical QML applications. The outcomes achieved in this study highlight that a quantum approach provides uplift over classical approaches as evidenced by the accuracy rates in classifying complex medical images. This provides a compelling case for the QCNN model's efficacy.

The findings of this research contribute to the growing body of knowledge on the applicability of QML in solving real-world problems, particularly in medical diagnostics. In addition, this opens up new possibilities for future research, including the potential to explore other complex tasks.

In conclusion, this study advances our understanding of QCNNs and demonstrates their practical application in a critical field. The promising results pave the way for further exploration and development of QML solutions in medical imaging, potentially significantly enhancing diagnostic accuracy and patient outcomes.

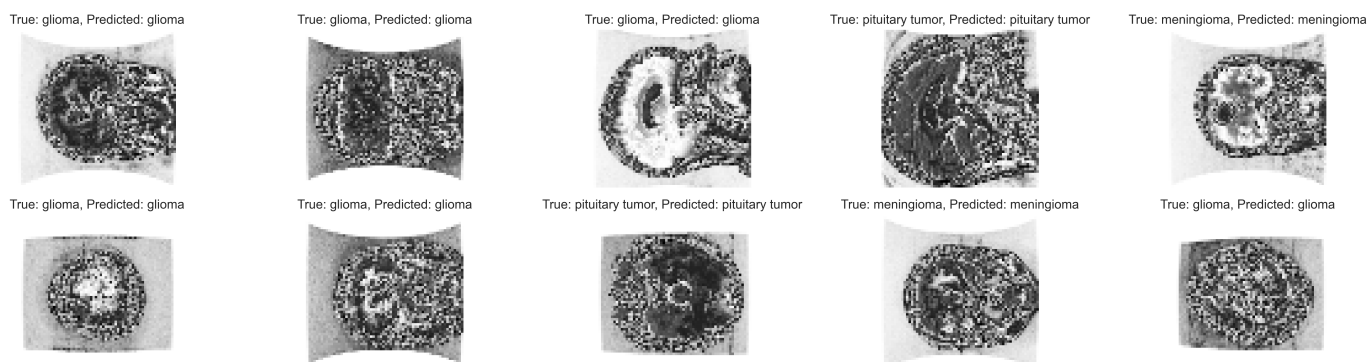


Fig. 8: Sample predictions with true and predicted labels.

DECLARATIONS

Conflicts of Interest

The authors declare no competing interests.

Authors' contributions

All authors have contributed equally.

Availability of Data and Materials

The datasets and numerical details necessary to replicate this work are available from the corresponding author upon reasonable request.

REFERENCES

- Siegel, R. L., Giaquinto, A. N., & Jemal, A. (2024). "Cancer statistics, 2024". *CA: A Cancer Journal for Clinicians*, <https://doi.org/10.3322/caac.21820>.
- Ullah, U., & Garcia-Zapirain, B. (2024). "Quantum Machine Learning Revolution in Healthcare: A Systematic Review of Emerging Perspectives and Applications". *IEEE Access*, <https://doi.org/10.1109/ACCESS.2024.3353461>.
- Vatandoost, M., & Litkouhi, S. (2019). "The future of healthcare facilities: how technology and medical advances may shape hospitals of the future". *Hospital Practices and Research*, *4*(1), <https://doi.org/10.15171/hpr.2019.01>.
- Menegatti, D., et al. (2023). "CADUCEO: A Platform to Support Federated Healthcare Facilities through Artificial Intelligence". *Healthcare*, *11*(15), <https://doi.org/10.3390/healthcare11152199>.
- Cao, Y., Romero, J., & Aspuru-Guzik, A. (2018). "Potential of quantum computing for drug discovery". *IBM Journal of Research and Development*, *62*(6), <https://doi.org/10.1147/JRD.2018.2888987>.
- Blunt, N. S., et al. (2022). "Perspective on the current state-of-the-art of quantum computing for drug discovery applications". *Journal of Chemical Theory and Computation*, *18*(12), <https://doi.org/10.1021/acs.jctc.2c00574>.
- Zinner, M., Dahlhausen, F., Boehme, P., Ehlers, J., Bieske, L., & Fehring, L. (2021). "Quantum computing's potential for drug discovery: Early stage industry dynamics." *Drug Discovery Today*, *26*(7), <https://doi.org/10.1016/j.drudis.2021.06.003>.
- Wang, P. H., Chen, J. H., Yang, Y. Y., Lee, C., & Tseng, Y. J. (2023). "Recent Advances in Quantum Computing for Drug Discovery and Development". *IEEE Nanotechnology Magazine*, <https://doi.org/10.1109/MNANO.2023.3249499>.
- Batra, K., Zorn, K. M., Foil, D. H., Minerali, E., Gawriljuk, V. O., Lane, T. R., & Ekins, S. (2021). "Quantum machine learning algorithms for drug discovery applications". *Journal of Chemical Information and Modeling*, *61*(6), <https://doi.org/10.1021/acs.jcim.1c00166>.
- Bauer, B., Bravyi, S., Motta, M., & Chan, G. K. L. (2020). "Quantum algorithms for quantum chemistry and quantum materials science". *Chemical Reviews*, *120*(22), <https://doi.org/10.1021/acs.chemrev.9b00829>.
- Liu, H., Low, G. H., Steiger, D. S., Häner, T., Reiher, M., & Troyer, M. (2022). "Prospects of quantum computing for molecular sciences". *Materials Theory*, *6*(1), <https://doi.org/10.1186/s41313-021-00039-z>.
- Smith, A., Kim, M. S., Pollmann, F., & Knolle, J. (2019). "Simulating quantum many-body dynamics on a current digital quantum computer". *npj Quantum Information*, *5*(1), <https://doi.org/10.1038/s41534-019-0217-0>.
- Micheletti, C., Hauke, P., & Faccioli, P. (2021). "Polymer physics by quantum computing". *Physical Review Letters*, *127*(8), <https://link.aps.org/doi/10.1103/PhysRevLett.127.080501>.
- Innan, N., Khan, M. A. Z., & Bennai, M. (2024). "Quantum computing for electronic structure analysis: Ground state energy and molecular properties calculations". *Materials Today Communications*, *38*(107760), <https://doi.org/10.1016/j.mtcomm.2023.107760>.
- Vorwerk, C., Sheng, N., Govoni, M., Huang, B., & Galli, G. (2022). "Quantum embedding theories to simulate condensed systems on quantum computers". *Nature Computational Science*, *2*(7), <https://doi.org/10.1038/s43588-022-00279-0>.
- Ajagekar, A., & You, F. (2019). "Quantum computing for energy systems optimization: Challenges and opportunities". *Energy*, *179*, <https://doi.org/10.1016/j.energy.2019.04.186>.
- Ajagekar, A., Humble, T., & You, F. (2020). "Quantum computing based hybrid solution strategies for large-scale discrete-continuous optimization problems." *Computers & Chemical Engineering*, *132*, <https://doi.org/10.1016/j.compchemeng.2019.106630>.
- Wang, L., Tang, F., & Wu, H. (2005). "Hybrid genetic algorithm based on quantum computing for numerical optimization and parameter estimation". *Applied Mathematics and Computation*, *171*(2), <https://doi.org/10.1016/j.amc.2005.01.115>.
- Shukla, A., & Vedula, P. (2019). "Trajectory optimization using quantum computing". *Journal of Global Optimization*, *75*, <https://doi.org/10.1007/s10898-019-00754-5>.
- Li, Y., Tian, M., Liu, G., Peng, C., & Jiao, L. (2020). "Quantum optimization and quantum learning: A survey". *Ieee Access*, *8*, <https://doi.org/10.1109/ACCESS.2020.3249499>.
- Orús, R., Mugel, S., & Lizaso, E. (2019). "Quantum computing for finance: Overview and prospects". *Reviews in Physics*, *4*, <https://doi.org/10.1016/j.revip.2019.100028>.
- Innan, N., Khan, M. A. Z., & Bennai, M. (2023). "Financial fraud detection: a comparative study of quantum machine learning models". *International Journal of Quantum Information*, <https://doi.org/10.1142/S0219749923500442>.
- Emmanoulopoulos, D., & Dimoska, S. (2022). "Quantum machine learning in finance: Time series forecasting". *arXiv preprint arXiv:2202.00599*.
- Herman, D., et al. (2022). "A survey of quantum computing for finance". *arXiv preprint arXiv:2201.02773*.
- Innan, N. et al. (2023). "Financial fraud detection using quantum graph neural networks". *arXiv preprint arXiv:2309.01127*.
- Correll, R., Weinberg, S. J., Sanches, F., Ide, T., & Suzuki, T. (2023). "Quantum Neural Networks for a Supply Chain Logistics Application". *Advanced Quantum Technologies*, *6*(7), <https://doi.org/10.1002/ajq.202200183>.
- Weinberg, S. J., Sanches, F., Ide, T., Kamiya, K., & Correll, R. (2023). "Supply chain logistics with quantum and classical annealing algorithms". *Scientific Reports*, *13*(1), <https://doi.org/10.1038/s41598-023-31765-8>.

- 28 Azzaoui, A. E., Kim, T. W., Pan, Y., & Park, J. H. (2021). "A quantum approximate optimization algorithm based on blockchain heuristic approach for scalable and secure smart logistics systems". *Human-centric Computing and Information Sciences*, **11**(46).
- 29 Gachnang, P., Ehrental, J., Hanne, T., & Dornberger, R. (2022). "Quantum Computing in Supply Chain Management State of the Art and Research Directions". *Asian Journal of Logistics Management*, **1**(1), <https://doi.org/10.14710/ajlm.2022.14325>.
- 30 Dixit, V., et al. (2021). "Training a quantum annealing based restricted boltzmann machine on cybersecurity data". *IEEE Transactions on Emerging Topics in Computational Intelligence*, **6**(3), <https://doi.org/10.1109/TETCI.2021.3074916>.
- 31 Suryotrisongko, H., & Musashi, Y. (2022). "Evaluating hybrid quantum-classical deep learning for cybersecurity botnet DGA detection". *Procedia Computer Science*, **197**, <https://doi.org/10.1016/j.procs.2021.12.135>.
- 32 Innan, N., et al.(2023). "Quantum State Tomography using Quantum Machine Learning". *arXiv preprint*, [arXiv:2308.10327](https://arxiv.org/abs/2308.10327).
- 33 Innan, N., & Khan, M. A. Z. (2023). "Classical-to-Quantum Sequence Encoding in Genomics". *arXiv preprint*, [arXiv:2304.10786](https://arxiv.org/abs/2304.10786).
- 34 Innan, N., & Bennai, M. (2023). "Simulation of a Variational Quantum Perceptron using Grover's Algorithm". *arXiv preprint*, [arXiv:2305.11040](https://arxiv.org/abs/2305.11040).
- 35 Innan, N., Khan M. A. Z., & Bennai, M. (2023). "Enhancing quantum support vector machines through variational kernel training". *Quantum Information Processing*, **22**(374), <https://doi.org/10.1007/s11128-023-04138-3>.
- 36 Dong, Y., Fu, Y., Liu, H., Che, X., Sun, L., & Luo, Y. (2023). "An improved hybrid quantum-classical convolutional neural network for multi-class brain tumor MRI classification". *Journal of Applied Physics*, **133**(6), <https://doi.org/10.1063/5.0138021>.
- 37 Amin, J., Anjum, M. A., Sharif, M., Jabeen, S., Kadry, S., & Moreno Ger, P. (2022). "A new model for brain tumor detection using ensemble transfer learning and quantum variational classifier". *Computational Intelligence and Neuroscience*, <https://doi.org/10.1155/2022/3236305>.
- 38 Amin, J., Anjum, M. A., Gul, N., & Sharif, M. (2022). "A secure two-qubit quantum model for segmentation and classification of brain tumor using MRI images based on blockchain." *Neural Computing and Applications*, **34**(20), <https://doi.org/10.1007/s00521-022-07388-x>.
- 39 Chandra, S., Saxena, S., Kumar, S., Chaube, M. K., & Bodhey, N. K. (2022, December). "A Novel Framework For Brain Disease Classification Using Quantum Convolutional Neural Network." *2022 IEEE International Women in Engineering (WIE) Conference on Electrical and Computer Engineering (WIECON-ECE)*, <https://doi.org/10.1109/WIECON-ECE57977.2022.10150851>.
- 40 Felefly, T. et al. (2023). "An Explainable MRI-Radiomic Quantum Neural Network to Differentiate Between Large Brain Metastases and High-Grade Glioma Using Quantum Annealing for Feature Selection." *Journal of Digital Imaging*, **36**(6), <https://doi.org/10.1007/s10278-023-00886-x>.
- 41 Konar, D., Bhattacharyya, S., Panigrahi, B. K., & Behrman, E. C. (2022). "Qutrit-Inspired Fully Self-Supervised Shallow Quantum Learning Network for Brain Tumor Segmentation." *IEEE Transactions on Neural Networks and Learning Systems*, **33**(11), <https://doi.org/10.1109/TNNLS.2021.3077188>.
- 42 Cheng, Jun. "Brain Tumor Dataset". *Figshare*. Dataset. (2017), <https://doi.org/10.6084/m9.figshare.1512427.v5>.
- 43 Cheng, Jun, et al. "Enhanced Performance of Brain Tumor Classification via Tumor Region Augmentation and Partition". *PLOS One*. pp. 10.10 (2015), <https://doi.org/10.1371/journal.pone.0140381>.
- 44 Cheng, Jun, et al. "Retrieval of Brain Tumors by Adaptive Spatial Pooling and Fisher Vector Representation." *PLOS One*. pp. 11.6 (2016), <https://doi.org/10.1371/journal.pone.0157112>.
- 45 Bergholm, Ville, et al. "Pennylane: Automatic differentiation of hybrid quantum-classical computations." *arXiv*, (2018), <https://arxiv.org/abs/1811.04968>.